Low Temperature Physics/Fizika Nizkikh Temperatur, 2019, v. 45, No. 7, pp. 856–861

Luminescence of molecular nitrogen in cryogenic plasmas

R.E. Boltnev[1,2,3], I.B. Bykhalo[1], V.V. Khmelenko[4], I.N. Krushinskaya[1], D.M. Lee[4], P.T. McColgan[4], S. Sheludiakov[4], and A.A. Pelmenev[1]

[1]*Branch of Talroze Institute for Energy Problems of Chemical Physics, Russian Academy of Sciences, Chernogolovka, 142432, Russia*

[2]*Joint Institute for High Temperatures, Russian Academy of Sciences, 13/2 Izhorskaya str., Moscow, 125412, Russia*

[3]*Moscow Institute of Physics and Technology, Dolgoprudnyi, Moscow region, 141701, Russia*

[4]*Institute for Quantum Science and Engineering, Department of Physics and Astronomy, Texas A&M University, College Station, Texas 77843, USA*

E-mail: boltnev@gmail.com

Received December 24, 2018, published online May 28, 2019

Great enhancement of molecular nitrogen luminescence in the afterglow of nitrogen-helium gas mixtures was observed at temperatures ≤ 10 K. The effect is explained by the increased efficiency of the recombination of nitrogen atoms and energy transfer from metastable nitrogen molecules and helium atoms to nitrogen molecules in the cold dense helium vapor.

Keywords: luminescence, molecular nitrogen, rotational structure, cryogenic plasma.

1. Introduction

The temperature of gas in non-equilibrium plasmas is often determined from the optical spectra by the rotational temperature estimation for emitting states of diatomic molecules [1–3]. It is well known that in non-thermal plasmas the rotational distribution in the emitting levels of the diatomic molecule may be out of equilibrium with the translational (gas) temperature. Then non-Boltzmann population distributions of rotational spectra are observed in non-equilibrium plasmas [1]. If equilibrium between translational and rotational degrees of freedom of molecules used as temperature probes is achieved, very good agreement of rotational temperatures with the real temperature of a buffer gas is usually obtained by using optical emission spectroscopy [2]. Envelopes of rotational spectra (or "synthetic" spectra) are frequently used to determine rotational temperatures of several hundred Kelvin and higher because of the very small values of the rotational constants (~ cm^{-1}) [2–6]. The situation is drastically changed for the case of cryogenic non-equilibrium plasmas with temperature ~ 1 K: rotational structures of molecular transitions are depleted and much simplified because only the lowest rotational levels of molecular states are populated [7–12]. Sometimes the temperature of a cryogenic plasma itself is very inhomogeneous due to either local heat release (corona or dc glow discharges, electron or proton beams) or plasma jets cooled with a buffer gas. Such local overheating can be successfully overcome in so-called "cryo-microplasmas" when the temperature is controlled by limiting the size of the discharge area with characteristic dimensions ~ 1 mm [13] or even less [14,15]. In the former case the full thermalization of NH_3 molecules with the helium buffer gas has been confirmed through rotationally resolved resonance enhanced multiphoton ionization spectra yielding a rotational temperature of 5 K, very close to the cell temperature of 3.8 K [13]. It is worth noting the existence of a "dark" mode of the direct current (dc) glow discharges at temperatures below 5 K: such plasmas do not emit light and the conductivity mechanism of the helium plasma is changed [16]. There are only a few experimental studies known involving such plasmas in the literature [17–20] up to the present time.

In this work we present new experimental results from a study of molecular nitrogen luminescence in cryogenic helium plasma jets. We have found that cooling a plasma jet to T ~ 10 K results in a significant enhancement of molecular nitrogen luminescence.

2. Experimental setup

The experimental setup has been described elsewhere [21]. The cryostat consists of two silvered-glass double-walled Dewars. The outer Dewar is filled with liquid nitrogen (LN_2), and the inner Dewar is filled with liquid helium (LHe). Temperatures of the liquid helium bath in the inner

Dewar down to 1.1 K are achievable with an Edwards model E2M80 rotary pump. Gas mixtures were prepared at room temperature using a gas handling system. In our experiments we used nitrogen–helium gas mixtures. Research-grade helium gas from Linde Electronics & Specialty Gases with 99.999% purity was used. The atomic source (Fig. 1(a)) is made of a cylindrical outer quartz tube with a concentric inner quartz capillary. At the bottom of the tube there are two electrodes, which surround the capillary. The tube is filled with liquid nitrogen, which simultaneously cools the incoming gas mixture and the discharge electrodes. The flux of $5\cdot10^{19}$ atoms/s of the nitrogen–helium mixture entering the cryostat was maintained by a Brooks Instrument 5850E flow controller. The gas mixture exits the radiofrequency discharge zone (rf discharge has a power of 60–80 W and a frequency of ~50 MHz) through an orifice with diameter 0.75 mm, which is 25 mm above the level of the He II inside the beaker. A pressure gradient of 2 Torr between discharge zone and a cold helium vapor creates a well-formed gas jet that penetrates the surface of the He II (Fig. 1(b)). The level of He II in the sample collection beaker was kept constant by filling with a thermomechanical fountain pump, which pumped He II from the bottom of the main bath.

Any emission of the plasma jet could be collected from any part of the jet by a lens focused onto the entrance of an optical bifurcated fiber. The fiber position (height) was determined by its distance from the He II level in the beaker. The bifurcated fiber splits into two separate channels, one of which was attached to an Ocean Optics spectrometer and the other to an Andor Shamrock SR500 spectrograph. The Ocean Optics spectrometer HR2000+ was used for detecting spectra over a broad wavelength range (200–1100 nm) with spectral resolution 1.3 nm, whereas the Andor spectrograph with a Newton EMCCD camera was used to obtain high resolution (0.05 nm) spectra. The plasma jet shown in Fig. 1(a) corresponds to a detuned rf discharge. Such a jet looks like a bright white beam. The jet temperature (at the top part of the jet) estimated from the rotational structure of very intense bands of the first negative system of N_2^+ is usually within the temperature range 120–180 K. In the case of a well-tuned rf discharge an orange color dominates at the top part of the jet and a green color dominates in the bottom part of the nitrogen–helium jet (Fig. 1(b)).

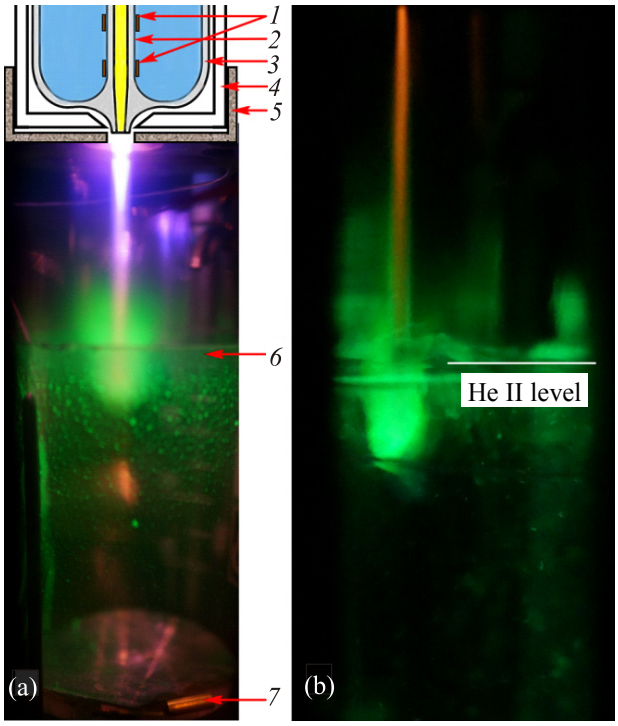

Fig. 1. (Color online) (a) Combined scheme of the plasma jet source, the jet, and the beaker filled with superfluid helium: *1* — discharge electrodes submerged in LN_2 (shown as a blue color); *2* — quartz capillary; *3* — quartz tube; *4* — vacuum jacket of the source; *5* — thermal shield; *6* — glass beaker filled with He II; *7* — thermometer in the beaker; (b) a plasma jet formed with a gas mixture $[N_2]/[He]$ = = 1/100 passed through a well tuned rf discharge.

3. Experimental results and discussion

Afterglow emission spectra of plasma jets formed by nitrogen–helium gas mixtures (with the N_2 content $\leq 1\%$) were studied upon fast cooling ($dT/dt \sim 10^5$ K/s) of the jets in the dense cold helium gas ($n_{He} \sim 10^{19}$ atoms/cm^3, $T \approx 1.5$ K). The molecular systems observed in the emission spectra shown in Figs. 2–5 are listed in the Table 1 as well as their traditional abbreviations, transitions and lifetimes.

We were able to observe the spectra of nitric oxide, NO, because of oxygen contamination in the helium gas at the level ~ 1 ppm. Addition of any impurity (more than 0.1%) to helium gas causes weakening and disappearance of the helium excimer He_2^* spectra in the plasma jet. Thus,

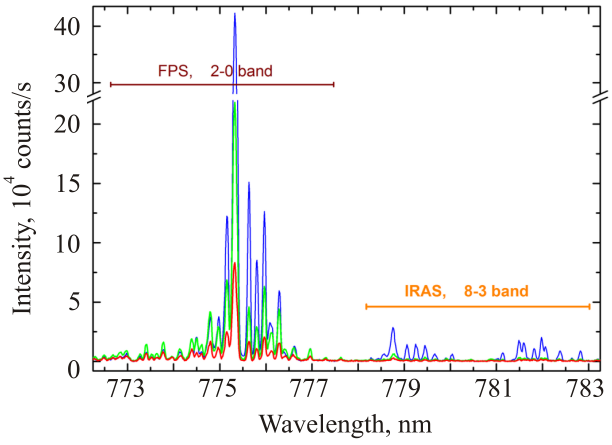

Fig. 2. (Color online) Comparison of molecular nitrogen spectra (the rotational structure of the 2–0 and 8–3 bands of the FPS and IRAS, see Table 1) detected from the top (red line), middle (green), and bottom (blue) parts of a plasma jet formed with gas mixture $[N_2]/[He]$ = 1/400.

Table 1. Molecular transitions observed in cold plasma jets

Molecule	System	Transition	Abbreviation	Lifetime of the upper state, μs
N_2	First positive	$B^3\Pi_g$–$A^3\Sigma_u^+$	FPS	≈ 10–12 [22]
N_2	Second positive	$C^3\Pi_u$–$B^3\Pi_g$	SPS	0.041 [23]
N_2	Goldstein–Kaplan	$C'^3\Pi_u$–$B^3\Pi_g$	GK	no data
N_2	Infrared afterglow	$B'^3\Sigma_u$– $B^3\Pi_g$	IRAS	25–50 [24]
N_2	Herman infrared	$C''^5\Pi_u$–$A^5\Sigma_g^+$	HIR	4.6 [25]
N_2	Gaydon–Herman green	$H^3\Phi_u$–$G^3\Delta_g$	GHG	0.028 [24]
N_2^+	First negative	$B^2\Sigma_u^+$–$X^2\Sigma_g^+$	FNS	0.062 [23]
NO	β	$B^2\Pi$ – $X^2\Pi$	β-system	2 [26]

the only helium lines observed in the spectra were those of atomic helium.

As one can see in Fig. 1(b), the emission intensity of the plasma jet increases just above the He II surface and inside a crater formed by the jet on the surface of liquid helium. This effect is shown in Fig. 2 by a comparison of rotational spectra of molecular nitrogen corresponding to the FPS 2–0 band and the IRAS 8–3 band detected from the top (red line), middle (green), and bottom (blue) parts of a plasma jet formed with gas mixture $[N_2]/[He] = 1/400$. The same parameters of the detection system (the slit widths, exposure time, and the distances between the jet, lens, and fiber) were used during the spectra registrations. Cooling the plasma jet down to $T \sim 10$ K drastically simplifies the rotational structures of molecular nitrogen transitions because of depletion of states with $J > 5$. Repopulation of rotational states is accompanied by an enhancement of the luminescence intensities of both bands observed (Fig. 2). Therefore, we can conclude that the higher concentrations of nitrogen molecules populating the $B'^3\Sigma_u^-(v = 8)$ and $B^3\Pi_g(v = 2)$ states, are *generated* in the coldest (bottom) part of a jet because their lifetimes (see the Table 1) are much shorter than the transit time of a particle in a jet, ~ 100 μs.

The other spectra of molecular nitrogen from the plasma jets shown in Figs. 3–5 were detected only in the bottom part of the jets.

From the spectra shown in Figs. 2–5 one can see that N_2, N_2^+, and NO molecules in the excited states were also detected in the bottom part of the plasma jets. Emission from very high vibrational levels (up to $v = 26$) of the $B^3\Pi_g$ state, corresponding to the FPS, was observed. The presence of excited N(^2D) and N(^2P) nitrogen atoms in the bottom part of the jets was revealed via the α- and δ-groups corresponding to the forbidden ^2D–^4S and ^2P–^2D transitions [27]. The appearance of these bands in the luminescence spectra of a jet provides us information on intense clustering occurring in the cold jet [28,29]. The transition ^2D–^4S is a doubly forbidden transition in the gas phase (the lifetime ~ 10^4 s), but the probability of the transition is greatly enhanced in a molecular nitrogen matrix [30]. Strong emission of N(^2D) atoms trapped in N_2 nanoclusters is shown in Fig. 6. The intense emission of the α-group from the bottom part of a jet provides evidence that the density of single nitrogen molecules in the jet is decreased due to their clustering. On the other hand, rather high densities of nitrogen atoms are present which emit after being trapped in the clusters. Therefore, we observed stronger emission of N_2

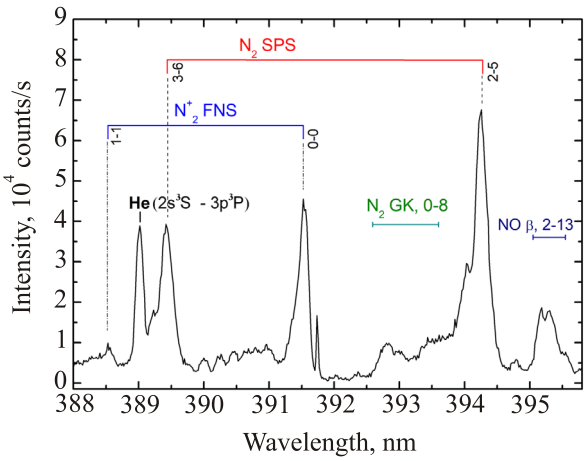

Fig. 3. Spectra of N_2 and NO molecules detected from the bottom part of the jet formed with gas mixture $[N_2]/[He] = 1/200$ passed through the rf discharge zone.

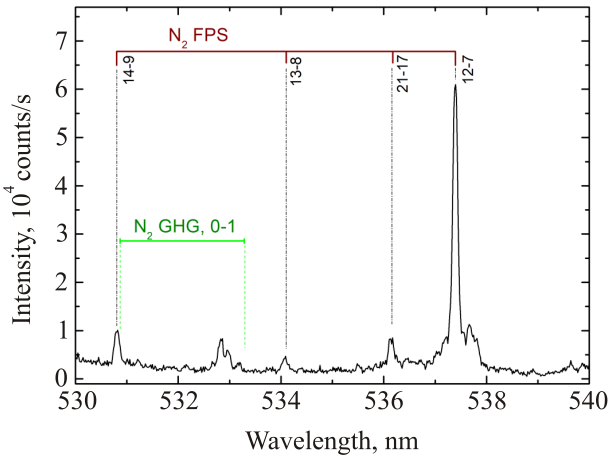

Fig. 4. Spectra of N_2 molecules detected from the bottom part of the jet formed when the gas mixture $[N_2]/[He] = 1/200$ passed through the rf discharge zone.

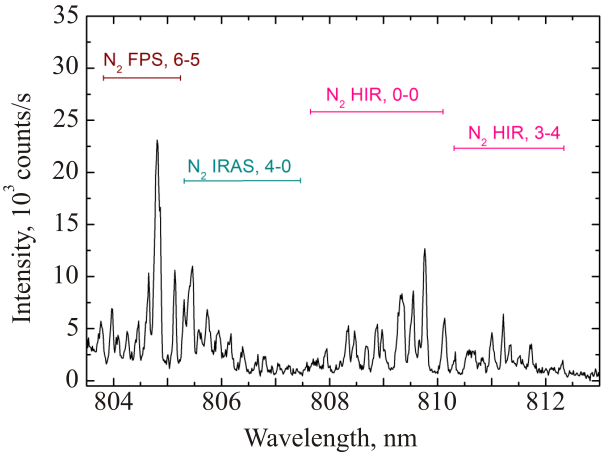

Fig. 5. Spectra of N_2 molecules detected for longer wavelengths from the bottom part of the jet formed when the gas mixture $[N_2]/[He] = 1/200$ passed through the rf discharge zone.

molecules (see Fig. 2) at their lower density in the coldest (bottom) part of the jet. Moreover, seven systems of molecular nitrogen (see Table 1) were observed in the afterglow of nitrogen–helium gas mixtures at temperatures ≤ 10 K due to both simplification of optical spectra (depletion of rotational structure) and intensity enhancement of molecular nitrogen luminescence. We should mention that the average travel time of an atom or molecule from the atomic source orifice to the He II surface is of order 100 μs. That means that all atoms and molecules excited in the discharge zone with lifetimes in the range 10–1000 ns should only emit light in the discharge zone and near the orifice. Therefore, excitation processes taking place in the jet are responsible for the observed molecular emission in the bottom part of a jet.

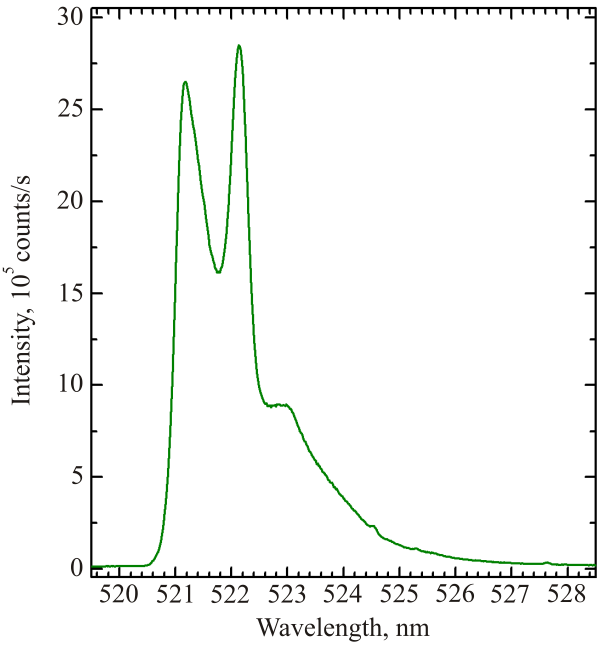

Fig. 6. Spectrum of the α-group of N atoms detected from the bottom part of a plasma jet formed with gas mixture $[N_2]/[He] = 1/200$.

The different processes resulting in formation of excited N_2 molecules in helium plasma are well studied. The formation of excited states of nitrogen molecules is a result of the Penning ionization of nitrogen molecules by He^* [31,32], He_2^* [33], and charge transfer reactions, with participation of ions He^+ and He_2^+ [34,35], followed by formation of N_2^+ ions and their recombination with electrons. On the other hand, cooling of a pure helium plasma leads to a significant increase in the concentration of metastable helium atoms, He^*, due to both their diffusion rate deceleration and the decrease in the rate of their "quenching" by helium atoms in the ground state [36,37]. The presence of metastable atoms He^* in the jet was proved by observation of the emission of helium atoms with the very short lifetimes of order 10 ns (Fig. 3). Such excited states of helium atoms can be populated through interactions of metastable He^* atoms in the jet.

Besides the previously mentioned helium excited species in helium–nitrogen plasmas, a very important role is played by metastable molecules $N_2(A^3\Sigma_u^+)$ which populate the $C'^3\Pi_u$ [38], $C^3\Pi_u$ [39], $C''^3\Pi_u$ [40,41], and $B^3\Pi_g$ [38] states through pooling reactions

$$N_2(A^3\Sigma_u^+, v) + N_2(A^3\Sigma_u^+, v) \rightarrow N_2(A^1X) + N_2^*.$$

The intersystem collisional transfer processes couple vibrational level populations of overlapping electronic low-lying triplet $A^3\Sigma_u^+$, $B^3\Pi_g$, $B'^3\Sigma_u^-$, and $C^3\Pi_u$ states [42]. Much less is known about a population mechanism for the high-lying state $H^3\Phi_u$ [43,44]. Nevertheless, we suggest that this state can be populated through recombination of two $N(^2D)$ atoms because the state correlates with the $N(^2D) + N(^2D)$ dissociation limit. Rather high concentrations of $N(^2D)$ atoms were revealed by observation of the intense α-group (Fig. 6) in the bottom part of a jet. It was theoretically predicted that at lower temperatures the $A^5\Sigma_g^+$ state of N_2 molecules is populated more efficiently due to recombination of nitrogen atoms in the ground state, $N(^4S)$: the rate constant for the formation the $A^5\Sigma_g^+$ state at $T = 4$ K is about one order of magnitude larger than that at 300 K [45]. The temperature in the bottom part of a plasma jet can be ≈ 10 K and, possibly, even lower in the crater. The metastable $A^5\Sigma_g^+$ state with the lifetime of 0.3 ms [46] is a precursor of the $B^3\Pi_g$ and $B'^3\Sigma_u^-$ states [45]. A rough estimation can be made from the results of ESR studies on the stabilization efficiency of $N(^4S)$ atoms in nanoclusters [47]. The highest density of $N(^4S)$ atoms in impurity–helium condensates may reach 10^{19} cm^{-3}. About of 1000 s is needed to accumulate 1 cm^3 of such a condensate. Thus the flux of $N(^4S)$ in the jet is $\leq 10^{16}$ at./s and the concentration $\leq 10^{16}/(7\cdot 10^3 \pi (0.2)^2) \sim 10^{13}$ at./cm^3, where the jet diameter 0.4 cm and velocity 70 m/s [48] were used. Therefore, the recombination of nitrogen atoms may give a valuable input into the N_2 luminescence enhancement.

Thus, we can conclude that great enhancement of molecular nitrogen luminescence in the afterglow of nitrogen–helium gas mixtures occurs due to high densities of energy carriers: metastable nitrogen molecules and helium atoms. Deceleration of a gas jet above the He II as well as decreasing of the thermal velocity of particles upon jet cooling provide a longer time for the recombination of nitrogen atoms, and the interaction of metastable particles with nitrogen molecules which both results in efficient excitation and the subsequent luminescence of nitrogen molecules.

4. Conclusions

1. Enhancement of molecular nitrogen luminescence was observed in the afterglow of nitrogen–helium gas mixtures at temperatures ≤ 10 K.

2. Up to seven systems of molecular nitrogen were observed in the afterglow of nitrogen–helium gas mixtures at temperatures ≤ 10 K due to simplification of optical spectra (depletion of rotational structure) and enhancement of molecular nitrogen luminescence.

3. The effect is explained by the increased efficiency of the recombination of nitrogen atoms and energy transfer from metastable nitrogen molecules and helium atoms to nitrogen molecules in the cold dense helium vapor.

Acknowledgments

This work was supported by NSF grant #DMR1707565.

1. P.J. Bruggeman, N. Sadeghi, D.C. Schram, and V. Linss, *Plasma Sources Sci. Technol.* **23**, 023001 (2014).
2. J. Zhang, L. Liu, T. Ma, and X. Deng, *Spectrochim. Acta A* **58**, 1915 (2002).
3. S.Y. Moon and W. Choe, *Spectrochim. Acta B* **58**, 249 (2003).
4. L. Robin, P. Vervisch, and B.G. Cheron, *Phys. Plasmas* **1**, 444 (1994).
5. C. Biloiu, X. Sun, Z. Harvey, and E. Scime, *J. Applied Phys.* **101**, 073303 (2007).
6. V.A. Shakhatov and Yu.A. Lebedev, *High Temp.* **50**, 658 (2012).
7. R.L. Brooks and J.L. Hunt, *J. Chem. Phys.* **89**, 7077 (1988).
8. A. Trottier, A.I. Jirasek, H.F. Tiedje, and R.L. Brooks, *Phys. Rev. A* **61**, 052504 (2000).
9. D.W. Tokaryk, G.R.Wagner, R.L. Brooks, J.L. Hunt, *J. Chem. Phys.* **103**, 10439 (1995).
10. Z. Li, N. Bonifaci, F. Aitken, K. von Haeften, V.M. Atrazhev, and V.A. Shakhatov, *IEEE TDEI* **16,** 742 (2009).
11. N. Bonifaci, V.M. Atrazhev, V.A. Shakhatov, R.E. Boltnev, K. Von Haeften, and J. Eloranta, *High Temp.* **55**, 326 (2017).
12. L.G. Mendoza-Luna, N.M.K. Shiltagh, M.J. Watkins, N. Bonifaci, F. Aitken, and K. von Haeften, *J. Phys. Chem. Lett.* **7**, 4666 (2016).
13. V. Singh, A.K. Samanta, N. Roth, D. Gusa, T. Ossenbrüggen, I. Rubinsky, D.A. Horke, and J. Küpper, *Phys. Rev. A* **97**, 032704 (2018).
14. S. Stauss, H. Muneoka, N. Ebato, F. Oshima, D.Z. Pai, and K. Terashima, *Plasma Sources Sci. Technol.* **22**, 025021 (2013).
15. K. Urabe, H. Muneoka, S. Stauss, O. Sakai, and K. Terashima, *Jap. J. Appl. Phys.* **54**, 106101 (2015).
16. E.I. Asinovskii, A.V. Kirillin, V.V. Markovets, and V.E. Fortov, *Dokl. Phys.* **46**, 321 (2001).
17. A.V. Kirillin and V.V. Markovets, *High Temp.* **11**, 637 (1973).
18. E.I. Asinovskii, A.V. Kirillin, and V.V. Markovets, *High Temp.* **13**, 858 (1975).
19. R.E. Boltnev, M.M. Vasiliev, E.A. Kononov, and O.F. Petrov, *J. Exp. Theor. Phys.* **126**, 561 (2018).
20. R.E. Boltnev, M.M. Vasiliev, and O.F. Petrov, *Instrum. Exp. Techniques* **61**, 626 (2018).
21. A. Meraki, S. Mao, P.T. McColgan, R.E. Boltnev, D.M. Lee, and V.V. Khmelenko, *J. Low Temp. Phys.* **185**, 269 (2016).
22. L.G. Piper, K.W. Holtzclaw, B.D. Green, and W.A.M. Blumberg, *J. Chem. Phys.* **90**, 5337 (1989).
23. F. Valk, M. Aints, P. Paris, T. Plank, J. Maksimov, and A. Tamm, *J. Phys. D: Appl. Phys.* **43**, 385202 (2010).
24. A. Lofthus and P.H. Krupenie, *J. Phys. Chem. Ref. Data* **6**, 113 (1977).
25. M. Hochlaf, H. Ndome, and D. Hammoutène, *J. Chem. Phys.* **132**, 104310 (2010).
26. J. Brzozowski, N. Elander, and P. Erman, *Phys. Scr.* **9**, 99 (1974).
27. R.E. Boltnev, I.B. Bykhalo, I.N. Krushinskaya, A.A. Pelmenev, V.V. Khmelenko, S. Mao, A. Meraki, S.C. Wilde, P.T. McColgan, and D.M. Lee, *J. Phys. Chem. A* **119**, 2438 (2015).
28. V. Kiryukhin, B. Keimer, R.E. Boltnev, V.V. Khmelenko, and E.B. Gordon, *Phys. Rev. Lett.* **79**, 1774 (1997).
29. V. Kiryukhin, E.P. Bernard, V.V. Khmelenko, R.E. Boltnev, N.V. Krainyukova, and D.M. Lee, *Phys. Rev. Lett.* **98**, 195506 (2007).
30. P.L. Kunsch and K. Dressler, *J. Chem. Phys.* **68**, 2550 (1978).
31. W.C. Richardson and D.W. Setser, *J. Chem. Phys.* **58**, 1809 (1973).
32. F.W. Lee and C.B. Collins, *J. Chem. Phys.* **65**, 5189 (1976).
33. F.W. Lee and C.B. Collins, *J. Chem. Phys.* **67**, 2798 (1977).
34. L.G. Piper, L. Gundel, J.E. Velazco, and D.W. Setser, *J. Chem. Phys.* **62**, 3883 (1975).
35. F.W. Lee, C.B. Collins, and R.A. Waller, *J. Chem. Phys.* **65**, 1605 (1976).
36. I.Ya. Fugol' and P.L. Pakhomov, *JETP Lett.* **3**, 254 (1966).
37. I.Ya. Fugol' and P.L. Pakhomov, *J. Exp. Theor. Phys.* **26**, 526 (1968).
38. G.N. Hays, C.J. Tracy, A.R. Demonchy, H.J. Oskam, *Chem. Phys. Lett.* **14**, 352 (1972).
39. G.N. Hays and H.J. Oskam, *J. Chem. Phys.* **59**, 6088 (1973).
40. I. Nadler, D.W. Setser, and S. Rosenvacs, *Chem. Phys. Lett.* **72**, 536 (1980).
41. L.G. Piper, *J. Chem. Phys.* **88**, 231 (1988).
42. J.S. Morrill and W.M.J. Benesch, *Geophys. Res.* **101**, 261 (1996).

43. P.K. Carroll, C.C. Collins, and J.T. Murnaghan, *J. Phys. B: Atom. Molec. Phys.* **5**, 1634 (1972).
44. M. Simek, V. Babicky, M. Clupek, and P. Sunka, *J. Phys. D: Appl. Phys.* **34,** 3185 (2001).
45. H. Partridge, S.R. Langhoff, and C.W. Bauschlicher, Jr., *J. Chem. Phys.* **88**, 3174 (1988).
46. W.J. Marinelli, W.J. Kessler, A.M. Woodward, and W.T. Rawlins, *J. Chem. Phys.* **92**, 1796 (1990).
47. A. Meraki, P.T. McColgan, R.E. Boltnev, D.M. Lee, and V.V. Khmelenko, *J. Low Tem. Phys.* **192**, 224 (2018).
48. E.A. Popov, J. Eloranta, J. Ahokas, and H. Kunttu, *Fiz. Nizk. Temp*. **29**, 684 (2003) [*Low Temp. Phys.* **29**, 510 (2003)].

Люмінесценція молекулярного азоту в кріогенній плазмі

Р.Є. Болтнєв, І.Б. Бихало, В.В. Хмеленко, І.М. Крушинська, D.M. Lee, P.T. McColgan, С. Шелудяков, А.А. Пельменьов

Значне посилення люмінесценції молекул азоту спостерігалося в післясвітінні азот-гелієвого газового струменя при температурі нижче 10 К. Даний ефект пояснено прискоренням рекомбінації атомів азоту і збільшенням ефективності передачі збудження від метастабільних молекул азоту і атомів гелію до молекул азоту в холодному газоподібному гелії.

Ключові слова: люмінесценція, молекулярний азот, ротаційна структура, кріоплазма.

Люминесценция молекулярного азота в криогенной плазме

Р.Е. Болтнев, И.Б. Быхало, В.В. Хмеленко, И.Н. Крушинская, D.M. Lee, P.T. McColgan, С. Шелудяков, А.А. Пельменёв

Значительное усиление люминесценции молекул азота наблюдалось в послесвечении азот-гелиевой газовой струи при температуре ниже 10 К. Данный эффект объяснен ускорением рекомбинации атомов азота и увеличением эффективности передачи возбуждения от метастабильных молекул азота и атомов гелия к молекулам азота в холодном газообразном гелии.

Ключевые слова: люминесценция, молекулярный азот, ротационная структура, криоплазма.